

RESEARCH PAPER

# Synthesis, Characterization, and Anticancer Bioactivity of a Novel Nano-Schiff Base Ligand (NPTIPPE) Derived from 4-Aminoantipyrine and Its Palladium Complex

Ashraf Abdulridha Hussein and Hayder Obaid Jamel \*

Department of Chemistry, College of Education, University of Al-Qadisiyah, Diwaniyah, Iraq

## ARTICLE INFO

### Article History:

Received 17 January 2025

Accepted 14 March 2025

Published 01 April 2025

### Keywords:

MCF-7 breast cancer cells

MTT assay

Palladium (II) complexes

Schiff-base nano ligand

(NPTIPPE)

## ABSTRACT

The novel nano ligand (NPTIPPE) was synthesized *via* a reaction sequence involving benzil, 4-aminoantipyrine, and 2-aminothiazole. Subsequently, the palladium (II) complex was formed by reacting NPTIPPE with palladium chloride in ethanol, maintaining a 1:1 metal:ligand ratio. The nano-ligand and its complex were characterized using various techniques, including NMR, FTIR, UV-Vis spectroscopy, FESEM, and XRD. The <sup>1</sup>H-NMR spectrum of NPTIPPE displayed signals corresponding to methyl and phenyl groups, while the <sup>13</sup>C-NMR spectrum identified signals associated with the pyrazole and thiazole rings. The FTIR spectra confirmed the presence of azomethine and aromatic groups, with shifts indicating coordination with palladium. The UV-Vis spectra revealed intra-ligand transitions and electronic transitions consistent with a square planar geometry for the palladium (II) complexes. Molar conductivity measurements suggested ionic characteristics. XRD analysis demonstrated differences in crystallite size and dislocation density between the nano ligand and complex. The FESEM images showed distinct morphological differences, reinforcing the structural findings. Biological evaluations using MTT assays on MCF-7 cancer cells and WRL-68 healthy cells indicated that the palladium (II) complexes exhibited higher cytotoxicity against cancer cells as compared to the ligand. The IC<sub>50</sub> values for the palladium (II) complex were 87.37 µg/mL for MCF-7 cells and 125.94 µg/mL for WRL-68 cells, suggesting its potential as an effective therapeutic agent against breast cancer.

## How to cite this article

Hussein A., Jamel H. Synthesis, Characterization, and Anticancer Bioactivity of a Novel Nano-Schiff Base Ligand (NPTIPPE) Derived from 4-Aminoantipyrine and Its Palladium Complex. J Nanostruct, 2025; 15(2):608-620. DOI: 10.22052/JNS.2025.02.021

## INTRODUCTION

1-phenyl-2,3-dimethylpyrazol-5-one is known as 4-aminoantipyrine or 4-aminophenazone. Pyrazole, a five-membered ring with two nitrogen atoms and a double bond, is important. Its substituted derivatives are biologically active [1, 2]. It also makes ion-selective electrodes [3] and suppresses enzymes [4]. The biological action

of 4-aminoantipyrine against bacteria makes it notable. It is a strong analgesic, anti-inflammatory, and fever reducer in circumstances where aspirin is unsuccessful, such as Hodgkin's disease and salicylate-resistant fevers. It also helps identify aromatic chemicals and metal ions utilizing various analytical methods. It helps make antipyrinyl azo

\* Corresponding Author Email: [haider.hassani@qu.edu.iq](mailto:haider.hassani@qu.edu.iq)



dyes, which are essential metal ion colorimetric indicators. Under acidic circumstances, these compounds produce metal chelate complexes. Certain pyrazole compounds have also shown promise against certain cancers [5]. Over 100 types of cancer result from the uncontrolled, fast, and deadly development of abnormal cells in organs and tissues [6, 7]. This disease is caused by DNA mutations in cells, which are organized into many genes with instructions for cellular functioning, growth, and division [7]. Incorrect instructions can cause the cell to stop working, causing numerous malignancies, including breast cancer, the most frequent disease in women after skin cancer [8]. Breast cancer usually starts in the milk-producing ducts (invasive ductal carcinoma), but it can also occur in the lobules or other breast tissues [9]. The new Schiff base ligand (NPTIPPE) generated from 4-aminoantipyrene and a pd (II) complex was synthesized in this study. These compounds were characterised spectroscopically and physically and tested for anticancer efficacy.

## MATERIALS AND METHODS

### Reagents and instruments

The chemicals used in this study were obtained from Merck, Sigma-Aldrich, and BDH. Breast cancer cell lines (MCF-7) and normal cell lines (WRL-68) were also obtained from the Educational

Research Center, Division of Cellular, Molecular, Microbial, and Animal Services / Roshdy Azmeh Company in Tehran. UV-Vis spectra in the range of 200–1000 nm were acquired using a Shimadzu UV-165 PCS spectrophotometer.  $^1\text{H}$  and  $^{13}\text{C}$ -NMR spectra were recorded at a frequency of 300 MHz using tetramethylsilane as an internal standard reference and DMSO- $d_6$  as a solvent. The FTIR spectra were recorded using a Shimadzu FTIR 8400S spectrophotometer in the range of 400-4000  $\text{cm}^{-1}$ . Melting points of the nano ligand and the prepared complex were determined using a Stuart melting point apparatus. Magnetic susceptibility measurements at room temperature were performed using a magnetic susceptibility balance model MSB-MKI. Flame atomic absorption spectra were recorded using a Shimadzu AA-6300. Elemental analysis for C, H, and N was conducted using an EA-300 elemental analyzer.

### Synthesis procedure

#### Synthesis of the heterocyclic Schiff base nano ligand (NPTIPPE)

The ligand (NPTIPPE) was synthesized in two steps. The first step involved the preparation of (4-(((2E,3E)-3-(hydroxy imino) butan-2-ylidene) amino) -1,5-dimethyl -2-phenyl- 1,2-dihydro -3H-pyrazol -3 - one (compound-A). This was achieved by reacting benzil (1.05 g, 0.005 mol) in

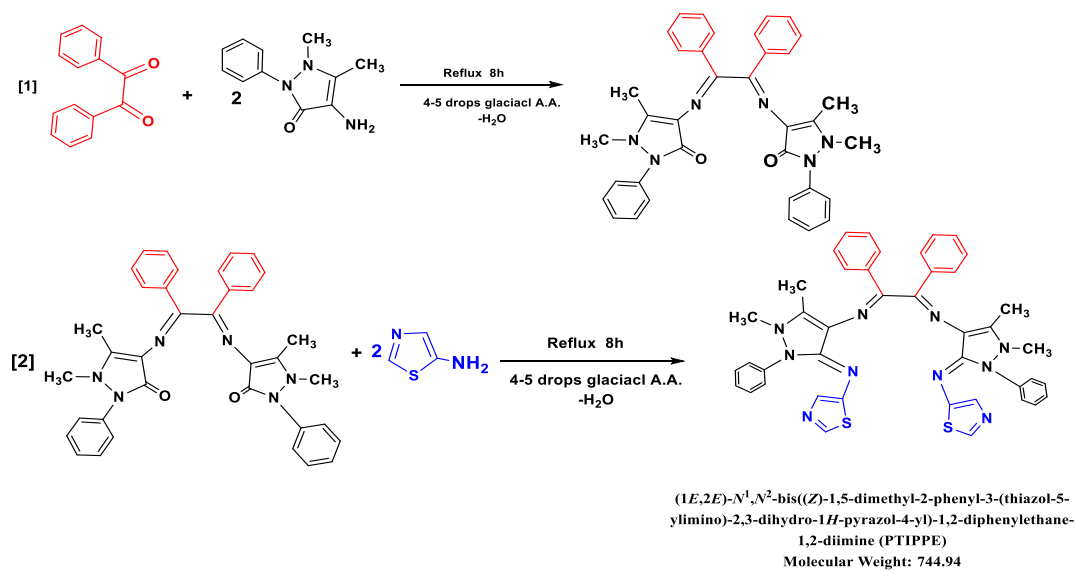


Fig. 1. Scheme for the synthesis of the novel schiff base nano ligand (NPTIPPE) derived from thiazole and salicylaldehyde.

25 mL of absolute ethanol, with the addition of 4-5 drops of glacial acetic acid. Simultaneously, 4-aminoantipyrine (2.03 g, 0.01 mol) was dissolved in 25 mL of absolute ethanol under continuous stirring. The mixture was then refluxed for 8 h, followed by cooling and collection. Recrystallization was performed by removing unreacted material using 98% ethanol. The resulting product was collected and weighed for use in the second step, yielding an 85% productivity. The nano ligand (1E,2E)-N1, N2-bis((Z)-1,5-dimethyl-2-phenyl-3-(thiazol-5-ylimino)-2,3-dihydro-1H-pyrazol-4-yl)-1,2-diphenylethane-1,2-diimine (NPTIPPE) was then prepared by dissolving compound-A (2.86 g, 0.01 mol) in 25 mL of absolute ethanol with continuous stirring and adding 4-5 drops of glacial

acetic acid. Separately, 2-aminothiazole (2 g, 0.02 mol) was dissolved in 25 mL of absolute ethanol. The solutions were mixed together and refluxed for 8 h. The mixture was cooled, and the resulting precipitate was filtered and dried. Recrystallization from absolute ethanol yielded a product with an 81% yield and a melting point of 120°C, as illustrated in Fig. 1.

#### Synthesis of the complex

The complex was prepared in a 1:1 ratio using a standard method. A solution of the nano ligand (NPTIPPE) (0.37 g, 0.001 mol) in 10 mL of ethanol was mixed with palladium chloride (PdCl<sub>2</sub>) (0.18 g, 0.001 mol) in 10 mL of absolute ethanol. The mixture was refluxed for 2 h with continuous

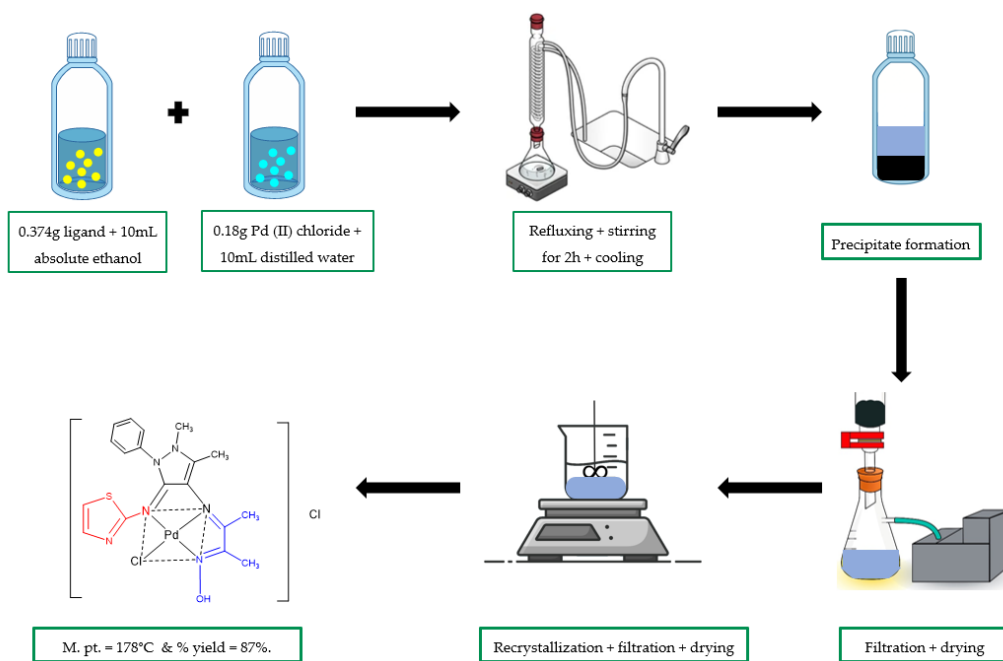


Fig. 2. Schematic illustration for the synthesis of Pd (II) complex by novel Schiff base nano ligand (NPTIPPE).

Table 1. Elemental analysis and some physical properties of the nano ligand (NPTIPPE) and its metallic complex.

| Compound<br>(Chemical Formula)  | Color       | M.P<br>(°C) | Yield<br>% | M.W<br>(g/mol) | Calc. (Found)% |              |                |                |                  |
|---|-------------|-------------|------------|----------------|----------------|--------------|----------------|----------------|------------------|
|   |             |             |            |                | C              | H            | N              | Pd             |                  |
| Ligand (NPTIPPE)<br>C <sub>18</sub> H <sub>20</sub> N <sub>6</sub> OS                     | Dark golden | 120         | 81         | 744.94         | 67.72<br>68.73 | 4.87<br>4.93 | 18.80<br>19.34 | -----<br>----- | -----<br>-----   |
| [Pd (NPTIPPE)Cl]Cl<br>C <sub>18</sub> H <sub>20</sub> Cl <sub>2</sub> N <sub>6</sub> OPdS | Brown       | 173         | 72         | 922.26         | 54.70<br>55.51 | 3.93<br>4.12 | 15.19<br>15.93 | 11.54<br>12.17 | 19.50<br>(20.17) |

stirring. It was then cooled, filtered, and dried before being recrystallized using absolute ethanol to obtain a pure complex. The yield was 72%, with a melting point of 173°C (Fig. 2).

#### Cell toxicity tests: cell lines and cultivation of MCF-7 breast cancer cell line

In this study, two cell lines were utilized: the breast cancer cell line (MCF-7) and the normal human liver cell line (WRL-68). The cell lines were stored in liquid nitrogen, maintained and tested at the Division of Cellular, Molecular, Microbial, and Animal Services / Roshdy Azmeh Company in Tehran. After preparing the cancer cell line suspensions (MCF-7) at a concentration of  $1 \times 10^5$  cells/well, the cell suspension was placed in a 96-well flat-bottom plate and incubated under appropriate conditions in an incubator containing 5% carbon dioxide (CO<sub>2</sub>) at 37°C for 24 h. Subsequently, 100  $\mu$ L of this suspension was added to each well. The prepared concentrations of the ligands and the Pd (II) complex—10, 25, 50, 100, 250, and 500  $\mu$ g/mL—were then added to the wells, with three wells per concentration. The plate was then incubated for 24 h at 37°C. Following this incubation, 10  $\mu$ L of MTT solution at a concentration of 0.45 mg/mL was added to each well, and the plate was incubated for an additional 4 h at 37°C. Afterward, 100  $\mu$ L of a DMSO solution was introduced into each well and left to incubate for duration of 5 min. Ultimately, the samples' absorbance was measured at a wavelength of 570 nm utilizing an ELISA reader. Subsequent statistical analysis was conducted on the optical density

measurements in order to get the IC<sub>50</sub> value.

## RESULTS AND DISCUSSION

The novel nano ligand (NPTIPPE) was synthesized through the sequential reaction of benzil with 4-aminoantipyrine and 2-aminothiazole. The Pd (II) complex was prepared by reacting the nano ligand (NPTIPPE) with palladium chloride dissolved in ethanol. Table 1 presents the physical properties and elemental analysis of both the ligand and its complex. The palladium complex was prepared in a 1:1 of metal:ligand ratio.

#### NMR spectrum of the novel Schiff base ligand (NPTIPPE)

Fig. 3 illustrates the <sup>1</sup>H-NMR spectrum of the ligand (NPTIPPE). The <sup>1</sup>H-NMR spectrum of the ligand (NPTIPPE) exhibited two singlets at  $\delta = 2.13$  ppm (S, 3H) and  $\delta = 3.16$  ppm (S, 3H), corresponding to the protons of the methyl groups (C-CH<sub>3</sub> and N-CH<sub>3</sub>) on the pyrazole ring, respectively [10]. Additional multiple signals were observed at  $\delta = 7.18 - 7.69$  ppm (M, 10H), attributed to the protons of the phenyl rings on the pyrazole and benzyl moieties [11]. The protons on the thiazole ring produced a doublet at  $\delta = 7.72$  and 7.75 ppm (d, 2H) [12].

#### <sup>13</sup>C-NMR spectrum of the ligand (NPTIPPE)

The <sup>13</sup>C-NMR spectrum of the ligand (NPTIPPE) showed a signal at 40.35 ppm due to DMSO. A signal at 10.43 ppm was observed (Fig. 4), corresponding to the carbon atoms (C8 and C39) of the methyl groups (-CH<sub>3</sub>) attached to the pyrazole

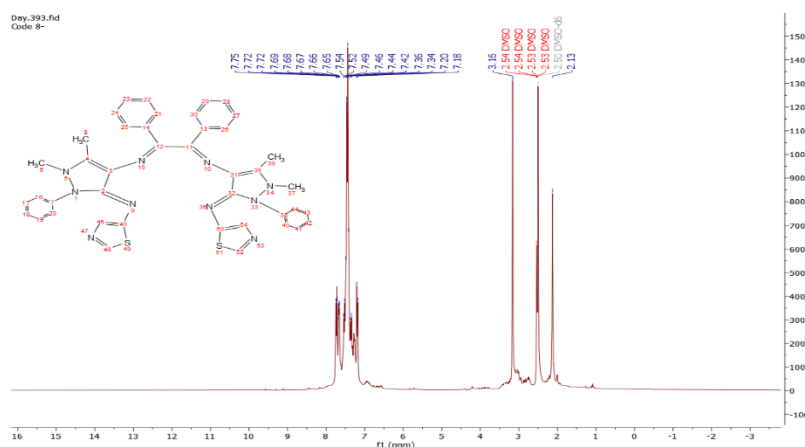


Fig. 3. <sup>1</sup>H-NMR result of the (NPTIPPE) ligand.



*UV-visible results*

The UV-Vis spectrum of the nano ligand (NPTIPPE) exhibited two peaks, as shown in Fig. 7 and Table 3. The first peak, centered at 243 nm ( $41152\text{ cm}^{-1}$ ), corresponds to the ( $\pi$ - $\pi^*$ ) transition, while the second peak, at 320 nm ( $31153\text{ cm}^{-1}$ ), is attributed to the ( $n$ - $\pi^*$ ) transition of the azomethine group [35, 38, 39]. In the UV-Vis spectrum of the palladium (II) complex (Fig. 8), several absorption peaks were observed at 252 nm ( $39683\text{ cm}^{-1}$ ) and 341 nm ( $29326\text{ cm}^{-1}$ ), indicating intra-ligand transitions. Three additional absorption peaks appeared at 478 nm ( $20921\text{ cm}^{-1}$ ), 508 nm ( $19685\text{ cm}^{-1}$ ), and 536 nm ( $18657\text{ cm}^{-1}$ ), corresponding to the electronic transitions  $^1A_{1g} \rightarrow ^1E_g$ ,  $^1A_{1g} \rightarrow ^1B_{1g}$ , and  $1A_{1g} \rightarrow ^1A_{2g}$ , respectively, confirming the square planar geometry of the complex [40]. Magnetic susceptibility measurements indicated

that the complex exhibits diamagnetic properties [41].

*Molar conductivity measurements*

Molar conductivity measurements were prepared using absolute ethanol at a concentration of  $1 \times 10^{-3}\text{ M}$  at room temperature. These measurements indicated that the prepared complex has a molar conductivity value of  $73.98\text{ ohm}^{-1}\text{ cm}^2\text{ mol}^{-1}$ , suggesting that the complex possesses ionic characteristics with a 1:2 ratio [42].

*XRD analysis*

A solid-state XRD study examined the crystal structure [22, 23] of NPTIPPE and its metal complexes in the  $2\theta=5$ -80 range. This investigation measured crystal structure, crystallite size, macrostrains, and dislocation density to determine

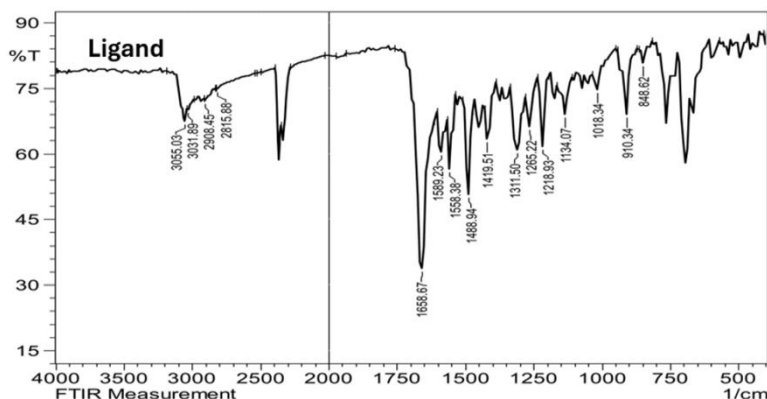


Fig. 5. FTIR spectrum of the NPTIPPE ligand.

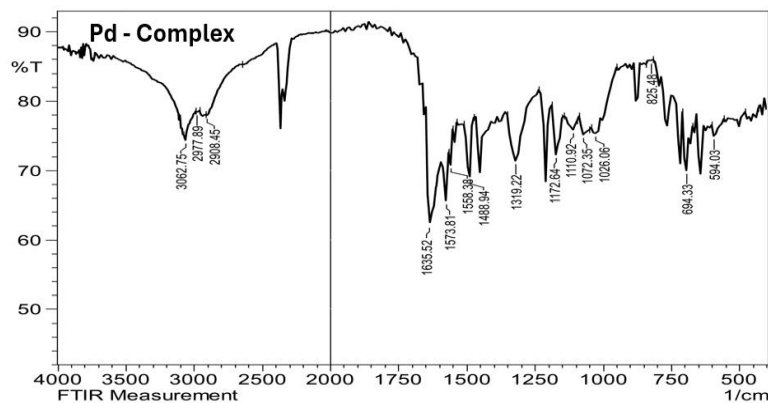


Fig. 6. FTIR spectrum of the Pd (II) complex.

purity and defects when the ligand is transformed into the palladium complex. Micro-strains such lattice deformation and crystal fracture due to crystal distortions, crystallite size, and

distribution cause some diffraction peaks [43-47]. The synthesized ligand's XRD pattern displayed strong peaks, indicating a crystalline network. In contrast, the palladium complex had broad peaks,

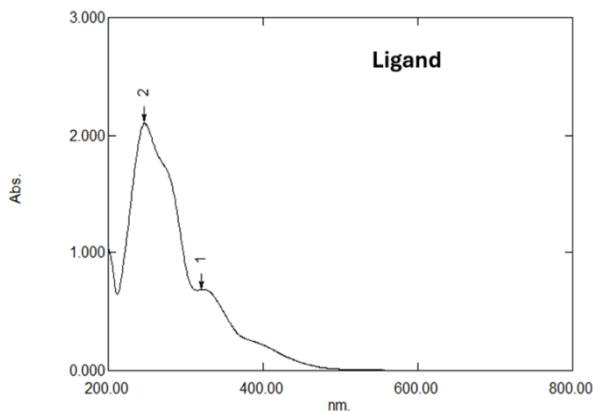


Fig. 7. UV-visible spectrum of the NPTIPPE ligand.

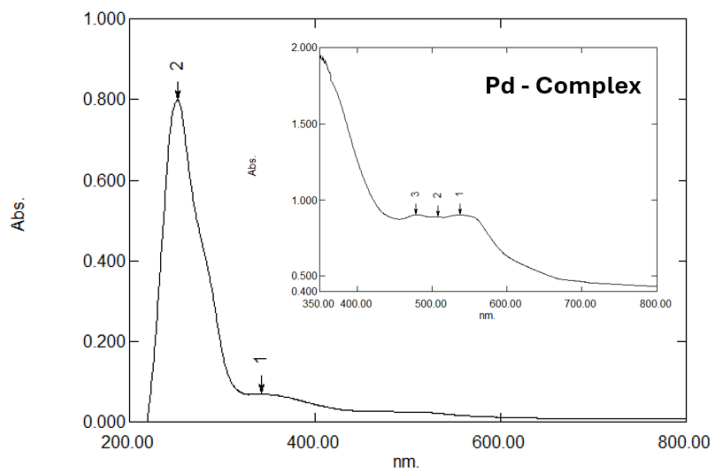


Fig. 8. UV-visible spectrum of the Pd (II) complex.

Table 3. Peaks absorption values, magnetic momentum and expected geometry for nano ligand (NPTIPPE) and Pd(II) complex.

| Compounds                     | $\lambda$ (nm) | $\nu$ ( $\text{cm}^{-1}$ ) | Transitions                     | $\mu_{\text{eff}}$ (B.M) | Geometry                          |
|-------------------------------|----------------|----------------------------|---------------------------------|--------------------------|-----------------------------------|
| Nano ligand (NPTIPPE )        | 243            | 41152                      | $\pi-\pi^*$                     | -                        | -                                 |
|                               | 321            | 31153                      | $n-\pi^*$                       |                          |                                   |
| [Pd (NPTIPPE)]Cl <sub>2</sub> | 252            | 39683                      | Intra Ligand                    | (Dia.)                   | Square planar<br>dsp <sup>2</sup> |
|                               | 341            | 29326                      | Intra Ligand                    |                          |                                   |
|                               | 478            | 20921                      | $^1A_{1g} \rightarrow ^1E_g$    |                          |                                   |
|                               | 508            | 19685                      | $^1A_{1g} \rightarrow ^1B_{1g}$ |                          |                                   |
|                               | 536            | 18657                      | $^1A_{1g} \rightarrow ^1A_{2g}$ |                          |                                   |

indicating amorphous structures. The sharpness of the peaks depends on the crystalline order, lattice properties, and crystal planes. Debye-Scherrer's equation was used to calculate the crystallite size of the nano ligand (NPTIPPE) and the palladium complex:

$$D = \frac{k \lambda}{\beta \cos \theta} \quad (1)$$

To calculate the dislocation density, the following equation is commonly used:

$$\delta = 1/D^2 \quad (2)$$

By analyzing the XRD patterns, significant

differences in crystallite size, dislocation density, and interplanar spacing (d-spacing) between the nano ligand (NPTIPPE) and the prepared palladium complex were observed. These differences confirm the coordination process between the ligand and the palladium ion [48, 49]. In Fig. 9 and Table 4, a comparison of the intensity and positions of the obtained peaks with standard reference cards indicates that these peaks correspond to the original compounds from which the complexes were derived. However, there were also unusual peaks that did not match any known substances, suggesting that the compounds are new and have not been compared with various global standards [50]. Utilizing the XRD data, it was concluded that the prepared materials exhibit nanomaterial

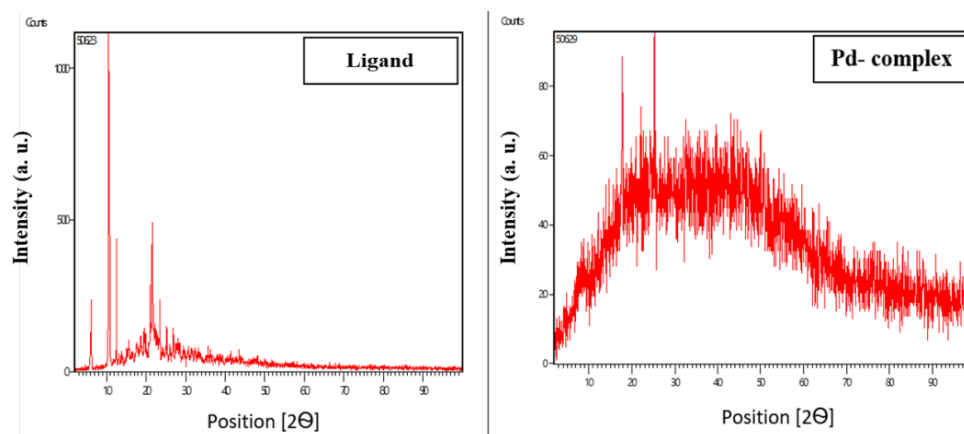


Fig. 9. XRD patterns of nano ligand (NPTIPPE) and Pd (II) complex.

Table 4. Summary of the information obtained from the XRD analysis i.e., diffraction angles, d-spacing, and relative intensities for ligand (NPTIPPE) and its Pd (II) complex.

| Compound                     | No. | Peak Position $2\theta$ | d-spacing (Å) | Rel.Int. [%] | FWHM | Width | Crystallite Size. (nm) | Lattice Strain |
|------------------------------|-----|-------------------------|---------------|--------------|------|-------|------------------------|----------------|
| Nano ligand (NPTIPPE)        | 1   | 0.04                    | 0.18          | 17.93        | 0.18 | 0.09  | 44.20                  | 0.04           |
|                              | 2   | 0.08                    | 0.21          | 100.00       | 0.21 | 0.10  | 38.54                  | 0.08           |
|                              | 3   | 0.04                    | 0.08          | 34.06        | 0.08 | 0.04  | 98.67                  | 0.04           |
|                              | 4   | 0.26                    | 0.32          | 35.15        | 0.32 | 0.16  | 25.35                  | 0.26           |
|                              | 5   | 0.18                    | 0.19          | 18.98        | 0.19 | 0.10  | 41.82                  | 0.18           |
| [Pd(NPTIPPE)]Cl <sub>2</sub> | 1   | 0.22                    | 0.32          | 93.86        | 0.32 | 0.16  | 24.97                  | 0.22           |
|                              | 2   | 22.01                   | 0.16          | 78.43        | 0.16 | 0.08  | 50.90                  | 0.13           |
|                              | 3   | 25.22                   | 0.23          | 100.00       | 0.23 | 0.12  | 35.24                  | 0.23           |
|                              | 4   | 43.08                   | 0.22          | 56.17        | 0.22 | 0.11  | 39.54                  | 0.37           |
|                              | 5   | 50.04                   | 0.16          | 69.48        | 0.16 | 0.08  | 55.49                  | 0.32           |

characteristics [51-53].

*Scanning electron microscopy (FE-SEM)*

As shown in Fig. 10, the surface investigations of resulting NPTIPPE and Pd(II) complex possess smooth shapes. It should be noted that Pd-complex reveals an interconnected structures as compared with NPTIPPE ligand.

*Anticancer activity*

The synthesized NPTIPPE and Pd(II) complex were evaluated for MTT on the most prevalent cancer cell line (MCF-7) (Figs. 11-14). To determine their therapeutic potential, NPTIPPE and Pd(II)

complex were evaluated on healthy WRL-68 liver cells. Following 24 h of incubation at 37°C, the MTT assay was performed at doses of 0, 10, 25, 50, 100, 250, and 500 µg/mL. The NPTIPPE effectively inhibited MCF-7 cancer and WRL-68 healthy cell growth, with the lowest inhibition at 10 µg/mL and the maximum at 500 µg/mL. The proportion of viable MCF-7 and WRL-68 cells after ligand contact ranged from 4.35924% to 92.94909% and 60.57843% to 99.06862%, respectively. Maximum MCF-7 cell inhibition was 95.64072% at 500 µg/mL, while WRL-68 cells showed 39.42157% inhibition. The ligand produced an IC50 value of 78.56 µg/mL for MCF-7 cells and 220.84 µg/mL for WRL-68

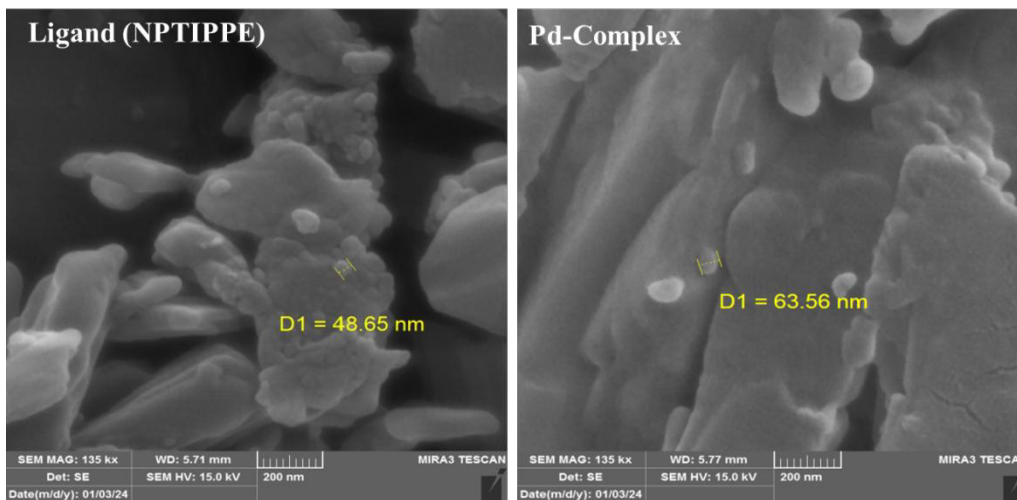


Fig. 10. The FESEM images of the synthesized NPTIPPE and Pd (II) complex.

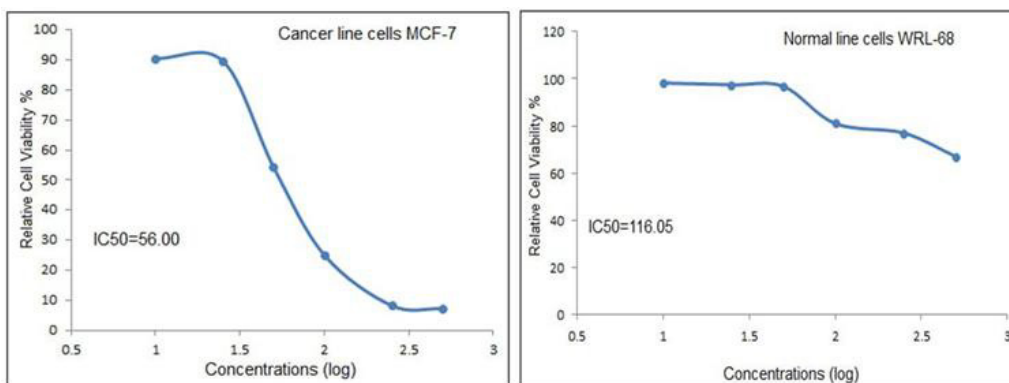


Fig. 11. The relationship between the biological activity of MCF-7 breast cancer cell line and WRL-68 normal cell line against the concentration of the ligand (NPTIPPE).

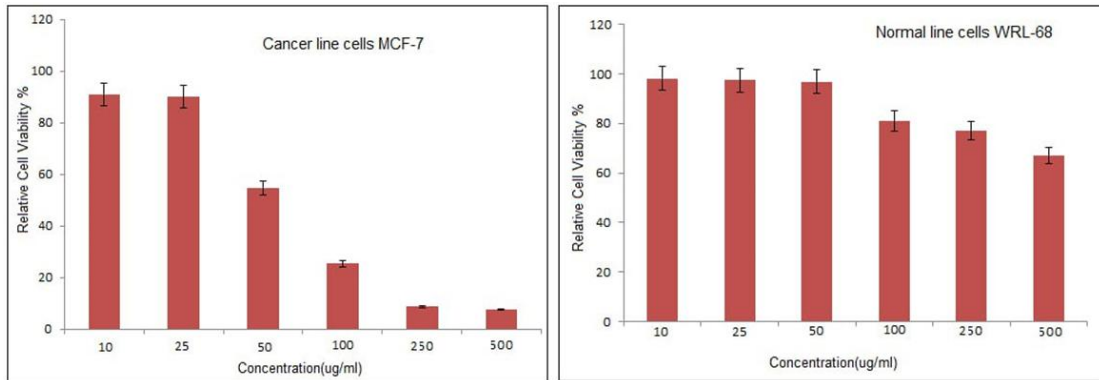


Fig. 12. Comparison of living cells at selected concentrations of the MCF-7 breast cancer cell line and WRL-68 normal cell line for the ligand (NPTIPPE).

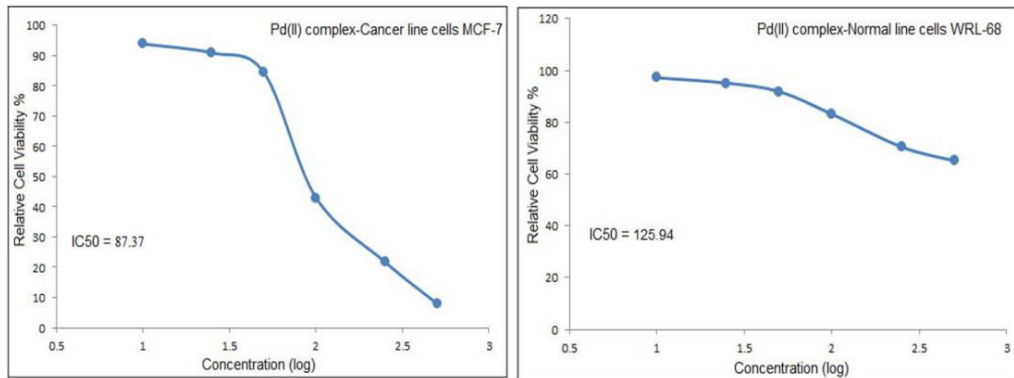


Fig. 13. The relationship between the biological activity of MCF-7 breast cancer cell line and WRL-68 normal cell line against the concentration of the Pd(II) complex.

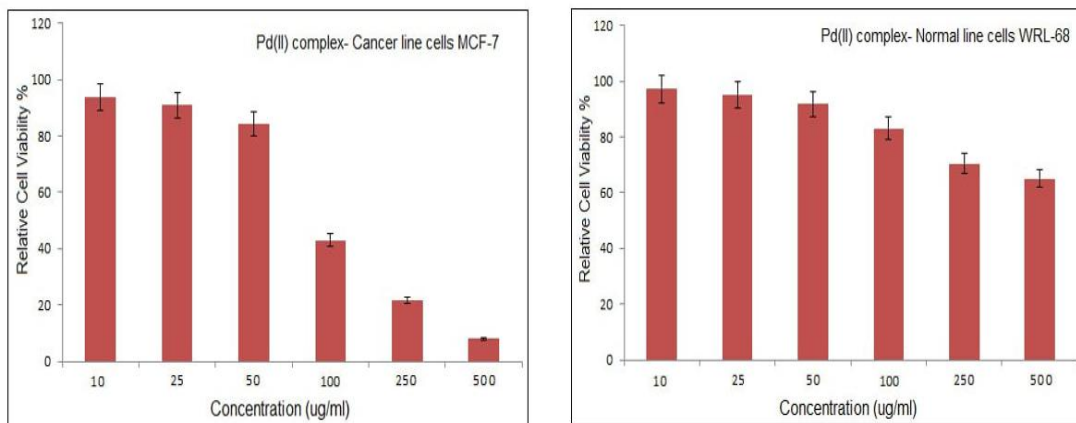


Fig. 14. Comparison of living cells at selected concentrations of the MCF-7 breast cancer cell line and WRL-68 normal cell line for the Pd(II) complex.

Table 5. Evaluation of the cytotoxicity of both the nano ligand against the MCF-7 cancer cell line and WRL-68 cell line after incubation (24 h) at 37 °C.

| Concentration ( $\mu\text{g/mL}$ ) | HL                      |       |                  |                          |        |                  |
|------------------------------------|-------------------------|-------|------------------|--------------------------|--------|------------------|
|                                    | Cancer line cells MCF-7 |       |                  | Normal line cells WRL-68 |        |                  |
|                                    | Cell Viability          |       | %Cell inhibition | Cell Viability           |        | %Cell inhibition |
|                                    | Mean                    | SD    |                  | Mean                     | SD     |                  |
| 10                                 | 92.949                  | 4.029 | 7.051            | 99.069                   | 1.274  | 0.931            |
| 25                                 | 91.486                  | 2.291 | 8.514            | 98.549                   | 15.958 | 1.451            |
| 50                                 | 79.111                  | 8.620 | 20.889           | 96.608                   | 3.571  | 3.392            |
| 100                                | 35.709                  | 4.274 | 64.291           | 78.578                   | 0.516  | 21.422           |
| 250                                | 21.781                  | 3.616 | 78.219           | 75.412                   | 4.710  | 24.588           |
| 500                                | 4.359                   | 0.101 | 95.641           | 60.578                   | 5.148  | 39.422           |
| IC50                               |                         | 78.56 |                  |                          | 220.84 |                  |

Table 6. Evaluation of the cytotoxicity of the Pd(II) complex against the MCF-7 cancer cell line and WRL-68 cell line after incubation (24 h) at 37 °C.

| Concentration ( $\mu\text{g/mL}$ ) | Pd(II) complex          |         |                  |                          |         |                  |
|------------------------------------|-------------------------|---------|------------------|--------------------------|---------|------------------|
|                                    | Cancer line cells MCF-7 |         |                  | Normal line cells WRL-68 |         |                  |
|                                    | Cell Viability          |         | %Cell inhibition | Cell Viability           |         | %Cell inhibition |
|                                    | Mean                    | SD      |                  | Mean                     | SD      |                  |
| 10                                 | 93.89225                | 5.13964 | 6.10775          | 97.18371                 | 5.02897 | 2.81629          |
| 25                                 | 90.92106                | 7.29320 | 9.07894          | 95.1072                  | 9.23502 | 4.8928           |
| 50                                 | 84.40449                | 1.69457 | 15.59551         | 91.85799                 | 6.64557 | 8.14201          |
| 100                                | 42.99023                | 4.25257 | 57.00977         | 83.13108                 | 1.27947 | 16.86892         |
| 250                                | 21.79632                | 3.64183 | 78.20368         | 70.47864                 | 9.65738 | 29.52136         |
| 500                                | 7.98046                 | 0.99631 | 92.01954         | 65.07944                 | 8.18448 | 34.92056         |
| IC50                               |                         | 87.37   |                  |                          | 125.94  |                  |

cells. The proliferation of MCF-7 cancer cells and WRL-68 healthy cells was inhibited by the Pd(II) complex of the NPTIPPE at concentrations ranging from 10  $\mu\text{g/mL}$  to 500  $\mu\text{g/mL}$ . After interaction with the Pd(II) complex, MCF-7 cells had 7.98046% to 93.89225% vitality and WRL-68 cells 65.07944% to 97.18371%. The maximum inhibition of MCF-7 cells was 92.01954% at 500  $\mu\text{g/mL}$ , while WRL-68 cells showed 34.92056% inhibition. IC50 values for palladium complex interaction with MCF-7 and WRL-68 cells were 87.37 and 125.94  $\mu\text{g/mL}$ , respectively (Table 5 and Table 6).

## CONCLUSION

In this study, a novel ligand (NPTIPPE) derived from antipyrine was synthesized in two steps, followed by the preparation of its palladium complex. Various methods were employed, including spectroscopic techniques (FTIR spectroscopy, UV-Vis. spectroscopy, and NMR spectroscopy), atomic absorption, FESEM, XRD, and physical methods (melting point, molar conductivity, elemental analysis) to confirm the

structure of the synthesized NPTIPPE and its complex. The FTIR spectrum showed that the ligand coordinates with the Pd (II) ion through the four nitrogen atoms of the azomethine groups, indicating that the ligand acts as a tetradentate ligand. This coordination results in a square planar geometry for the complex. MTT assays were conducted for both NPTIPPE and its palladium complex on cancerous and healthy cells. The palladium complex was found to be more effective against breast cancer cells (MCF-7) than the nano ligand itself, suggesting that the palladium complex holds significant potential as a therapeutic agent.

## CONFLICT OF INTEREST

The authors declare that there is no conflict of interests regarding the publication of this manuscript.

## REFERENCES

- Özbek O, Gürdere MB. Synthesis and anticancer properties of 2-aminothiazole derivatives. *Phosphorus, Sulfur, and Silicon and the Related Elements*. 2021;196(5):444-454.
- Synthesis and Characterization of Zinc(II), Cadmium(II) and

- Palladium(II) Complexes with the Thiophene-Derived Schiff Base Ligand. American Chemical Society (ACS).
- Zhang Z-H, Wu H-M, Deng S-N, Cai X-Y, Yao Y, Mwenda MC, et al. Design, Synthesis, and Anticancer Activities of Novel 2-Amino-4-phenylthiazole Scaffold Containing Amide Moieties. *Journal of Chemistry*. 2018;2018:1-8.
  - Mishra CB, Kumari S, Tiwari M. Thiazole: A promising heterocycle for the development of potent CNS active agents. *Eur J Med Chem*. 2015;92:1-34.
  - Forer A, Fabian L. Does 2,3-butanedione monoxime inhibit nonmuscle myosin? *Protoplasma*. 2005;225(1-2):1-4.
  - Shaker SA. Preparation and Spectral Properties of Mixed-Ligand Complexes of VO(IV), Ni(II), Zn(II), Pd(II), Cd(II) and Pb(II) with Dimethylglyoxime and N-acetylglycine. *Journal of Chemistry*. 2010;7(S1).
  - Hamad K, Kaseem M, Deri F. Recycling of waste from polymer materials: An overview of the recent works. *Polymer Degradation and Stability*. 2013;98(12):2801-2812.
  - Conn HW. *Laboratory Manual in General Microbiology*. By Ward Giltner. John Wiley and Sons. Pp. 418. \$2.50. Science. 1916;43(1119):823-823.
  - Advanced organic chemistry Third edition, by G. W. Wheland. Pp. xi + 871. John Wiley & Sons Inc., New York; John Wiley & Sons Ltd, London. 1960. E7 net. *Endeavour*. 1961;20(79):171.
  - Spinu C, Kriza A, Meghea A, Tigae C. Studies on N-[2-Thienylmethylidene]-2-Aminopyridine Complexes of Fe(II), Co(II), Ni(II), Cu(II), Zn(II) and Cd(II). *Southern Brazilian Journal of Chemistry*. 2001;9(10):17-22.
  - Lastovickova M, Strouhalova D, Bobalova J. Use of Lectin-based Affinity Techniques in Breast Cancer Glycoproteomics: A Review. *J Proteome Res*. 2020;19(5):1885-1899.
  - Jacobsson J. Superoxide dismutase in CSF from amyotrophic lateral sclerosis patients with and without CuZn-superoxide dismutase mutations. *Brain*. 2001;124(7):1461-1466.
  - Hansen S, Thiel S, Willis A, Holmskov U, Jensenius JC. Purification and Characterization of Two Mannan-Binding Lectins from Mouse Serum. *The Journal of Immunology*. 2000;164(5):2610-2618.
  - Yehia SM, Ayoub IM, Watanabe M, Devkota HP, Singab ANB. Metabolic profiling, antioxidant, and enzyme inhibition potential of *Iris pseudacorus* L. from Egypt and Japan: A comparative study. *Sci Rep*. 2023;13(1):5233-5233.
  - Hine J, Yeh CY. Equilibrium in formation and conformational isomerization of imines derived from isobutyraldehyde and saturated aliphatic primary amines. *Journal of the American Chemical Society*. 1967;89(11):2669-2676.
  - Sacarescu L, Ardeleanu R, Sacarescu G, Simionescu M. Highly Crosslinked Polysilane-Schiff Base. *Polym Bull*. 2005;54(1-2):29-37.
  - da Silva CM, da Silva DL, Modolo LV, Alves RB, de Resende MA, Martins CVB, et al. Schiff bases: A short review of their antimicrobial activities. *Journal of Advanced Research*. 2011;2(1):1-8.
  - Synthesis, Characterization And Antibacterial Analysis Of Benzocaine Schiff Base Metal Complexes. *Nanotechnology Perceptions*. 2024;20(6).
  - Abdul-Rida NA, Talib KM. New Chalcone Derivatives as Anticancer and Antioxidant Agents: Synthesis, Molecular Docking Study and Biological Evaluation. *Chemical Problems*. 2024;22(2):177-186.
  - Hamzah SK, Jabbar NK, Almzaial AJ, sabit RA. The Role Caspase-8 and DNA Methylation in patients with Ovarian Cancer: Relationship with Oxidative Stress and Inflammation. *Research Journal of Pharmacy and Technology*. 2021:2676-2680.
  - Pahonțu E, Ilieș D-C, Shova S, Paraschivescu C, Badea M, Gulea A, et al. Synthesis, characterization, crystal structure and antimicrobial activity of copper(II) complexes with the Schiff base derived from 2-hydroxy-4-methoxybenzaldehyde. *Molecules (Basel, Switzerland)*. 2015;20(4):5771-5792.
  - Batool M, Haider MN, Javed T. Applications of Spectroscopic Techniques for Characterization of Polymer Nanocomposite: A Review. *Journal of Inorganic and Organometallic Polymers and Materials*. 2022;32(12):4478-4503.
  - Majeed HJ, Idrees TJ, Mahdi MA, Abed MJ, Batool M, Yousefi SR, et al. Synthesis and application of novel sodium carboxymethyl cellulose-g-poly acrylic acid carbon dots hydrogel nanocomposite (NaCMC-g-PAAc/ CDs) for adsorptive removal of malachite green dye. *Desalination and Water Treatment*. 2024;320:100822.
  - Mahmood Taher A, Ali Kadhim Kyhoiesh H, Shakir Waheeb A, Al-Adilee KJ, Jasim LS. Synthesis, characterization, biological activity, and modelling protein docking of divalent, trivalent, and tetravalent metal ion complexes of new azo dye ligand (N,N,O) derived from benzimidazole. *Results in Chemistry*. 2024;12:101911.
  - Reddy GN, Losetty V, Reddy KR, Yadav CH, Sampath S. Synthesis, spectroscopic characterization, physicochemical properties, biological activity and docking study of Cu (II) and La (III) metal complexes with a Schiff base ligand. *Polyhedron*. 2023;244:116615.
  - Hiroki A, Taguchi M. Development of Environmentally Friendly Cellulose Derivative-Based Hydrogels for Contact Lenses Using a Radiation Crosslinking Technique. *Applied Sciences*. 2021;11(19):9168.
  - Ashraf MA, Wajid A, Mahmood K, Maah MJ, Yusoff I. Spectral Investigation of the Activities of AminoSubstituted Bases. *International Journal of Chemical Engineering and Applications*. 2011:252-255.
  - Jamel HO, Jasim MH, Mahdi MA, Ganduh SH, Batool M, Jasim LS, et al. Adsorption of Rhodamine B dye from solution using 3-((1-(4-((1H-benzo[d]imidazol-2-yl)amino)phenyl)ethylidene)amino)phenol (BIAPEHB)/ P(AA-co-AM) composite. *Desalination and Water Treatment*. 2025;321:101019.
  - Jasim LS, Aljeboree AM, Sahib IJ, Mahdi MA, Abdulrazzak FH, Alkaim AF. Effective adsorptive removal of riboflavin (RF) over activated carbon. *AIP Conference Proceedings: AIP Publishing*; 2022. p. 030030.
  - Applications and Risk Assessments of Ionic Liquids in Chemical and Pharmaceutical Domains: An Updated Overview. *Jordan Journal of Chemistry*. 2023;18(2):53-76.
  - Sahib IJ, Aljeboree AM, Mahdi AB, Jasim LS, Alkaim AF. Highly efficient removal of toxic Pb(II) from aqueous solution by chitosan-g-p(AA-co-AAm) hydrogel: Kinetic, models. *AIP Conference Proceedings: AIP Publishing*; 2023. p. 040073.
  - Jasim L, Radhy N, Jamel H. Synthesis and Characterization of Poly (Acryl Amide - Maleic Acid) Hydrogel: Adsorption Kinetics of a Malachite Green from Aqueous Solutions. *Eurasian Journal of Analytical Chemistry*. 2018;13(1b).
  - Jasim LS, Abdulsahib WK, Ganduh SH, Radia ND. New Approach for Sulfadiazine Toxicity Management using Carboxymethyl Cellulose Grafted Acrylamide Hydrogel. *International Journal of Drug Delivery Technology*. 2020;10(02):259-264.
  - Kareem Hamzah S. Study some biochemical parameters in pregnant women with hypertension. *Journal of Physics*:

- Conference Series. 2019;1234(1):012092.
35. Yasir AF, Jamel HO. Synthesis of a New DPTYEAP Ligand and Its Complexes with Their Assessments on Physical Properties, Antioxidant, and Biological Potential to Treat Breast Cancer. *Indonesian Journal of Chemistry*. 2023;23(3):796.
  36. Al-Masoudi NA, Kassim AG, Abdul-Reda NA. Synthesis of Potential Pyrimidine Derivatives via Suzuki Cross-Coupling Reaction as HIV and Kinesin Eg5 Inhibitors. *Nucleosides, Nucleotides and Nucleic Acids*. 2014;33(3):141-161.
  37. Nabeel AA-R, Adnan S, Jaber QAH. Development of Novel Imaging Fluorescent Agents Bearing Anti-Inflammatory Drugs: Synthesis, Structural Characterization and Evaluation of Biological Activity. *Russian Journal of Bioorganic Chemistry*. 2020;46(4):620-626.
  38. Mahde BW, Sultan AM, Mahdi MA, Jasim LS. Kinetic Adsorption and Release Study of Sulfadiazine Hydrochloride Drug from Aqueous Solutions on GO/P(AA-AM-MCC) Composite. *International Journal of Drug Delivery Technology*. 2022;12(04):1583-1589.
  39. Mahdi MA, Oroumi G, Samimi F, Dawi EA, Abed MJ, Alzaidy AH, et al. Tailoring the innovative Lu<sub>2</sub>CrMnO<sub>6</sub> double perovskite nanostructure as an efficient electrode materials for electrochemical hydrogen storage application. *Journal of Energy Storage*. 2024;88:111660.
  40. Maddila S, Gorle S, Seshadri N, Lavanya P, Jonnalagadda SB. Synthesis, antibacterial and antifungal activity of novel benzothiazole pyrimidine derivatives. *Arabian Journal of Chemistry*. 2016;9(5):681-687.
  41. Pluth MD, Tonzetich ZJ. Hydrosulfide complexes of the transition elements: diverse roles in bioinorganic, cluster, coordination, and organometallic chemistry. *Chem Soc Rev*. 2020;49(12):4070-4134.
  42. Jiang J, Tang X, Dou W, Zhang H, Liu W, Wang C, et al. Synthesis and characterization of the ligand based on benzoxazole and its transition metal complexes: DNA-binding and antitumor activity. *J Inorg Biochem*. 2010;104(5):583-591.
  43. Abouzied AS, Break MKB, Huwaimel B, Hussein W, Alafnan A, Younes KM. Discovery of A Novel Synthetic Thiazole-benzimidazole Conjugate that Acts as a Potent Pancreatic Lipase Inhibitor using in silico and in vitro Approaches. *Indian Journal of Pharmaceutical Education and Research*. 2023;57(1):218-227.
  44. Charisiadis P, Kontogianni VG, Tsiafoulis CG, Tzakos AG, Siskos M, Gerothanassis IP. <sup>1</sup>H-NMR as a structural and analytical tool of intra- and intermolecular hydrogen bonds of phenol-containing natural products and model compounds. *Molecules (Basel, Switzerland)*. 2014;19(9):13643-13682.
  45. Sajeesh S, Sharma CP. Mucoadhesive hydrogel microparticles based on poly (methacrylic acid-vinyl pyrrolidone)-chitosan for oral drug delivery. *Drug Deliv*. 2010;18(4):227-235.
  46. Kianipour S, Razavi FS, Hajizadeh-Oghaz M, Abdulsahib WK, Mahdi MA, Jasim LS, et al. The synthesis of the P/N-type NdCoO<sub>3</sub>/g-C<sub>3</sub>N<sub>4</sub> nano-heterojunction as a high-performance photocatalyst for the enhanced photocatalytic degradation of pollutants under visible-light irradiation. *Arabian Journal of Chemistry*. 2022;15(6):103840.
  47. Hosseini M, Ghanbari M, Dawi EA, Mahdi MA, Ganduh SH, Jasim LS, et al. Investigations of nickel silicate for degradation of water-soluble organic pollutants. *Int J Hydrogen Energy*. 2024;61:307-315.
  48. Mekhalif Z, Fonder G, Auguste D, Laffineur F, Delhalle J. Impact of the anchoring groups X (-SH, -S-S-, -SeH and -Se-Se-) of CF<sub>3</sub>(CF<sub>2</sub>)<sub>3</sub>(CH<sub>2</sub>)<sub>11</sub>x molecules self-assembled on oxidised electroplated copper. *J Electroanal Chem*. 2008;618(1-2):24-32.
  49. Venugopala KN, Chandrashekhara S, Pillay M, Bhandary S, Kandeel M, Mahomoodally FM, et al. Synthesis and Structural Elucidation of Novel Benzothiazole Derivatives as Anti-tubercular Agents: In-silico Screening for Possible Target Identification. *Medicinal Chemistry*. 2019;15(3):311-326.
  50. Issa YM, Hassib HB, Abdelaal HE. <sup>1</sup>H NMR, <sup>13</sup>C NMR and mass spectral studies of some Schiff bases derived from 3-amino-1,2,4-triazole. *Spectrochimica Acta Part A: Molecular and Biomolecular Spectroscopy*. 2009;74(4):902-910.
  51. Rang HP, Dale MM, Ritter JM, Flower RJ, Henderson G. Acknowledgements. Rang & Dale's Pharmacology: Elsevier; 2012. p. xvi.
  52. Spectrophotometric Determination of Metoclopramide-HCl in the standard raw and it compared with pharmaceuticals. *Journal of Pharmaceutical Negative Results*. 2021;21(2).
  53. Atyaa AI, Radhy ND, Jasim LS. Synthesis and Characterization of Graphene Oxide/Hydrogel Composites and Their Applications to Adsorptive Removal Congo Red from Aqueous Solution. *Journal of Physics: Conference Series*. 2019;1234(1):012095.